

# AutomaChef: A Physics-informed Demonstration-guided Learning Framework for Granular Material Manipulation

Minglun Wei<sup>1</sup>, Xintong Yang<sup>1</sup>, Yu-Kun Lai<sup>2</sup>, Seyed Amir Tafrihi<sup>1</sup> and Ze Ji<sup>1</sup>

**Abstract**—Due to the complex physical properties of granular materials, research on robot learning for manipulating such materials predominantly either disregards the consideration of their physical characteristics or uses surrogate models to approximate their physical properties. Learning to manipulate granular materials based on physical information obtained through precise modelling remains an unsolved problem. In this paper, we propose to address this challenge by constructing a differentiable physics simulator for granular materials based on the Taichi programming language and developing a learning framework accelerated by imperfect demonstrations that are generated via gradient-based optimisation on non-granular materials through our simulator. Experimental results show that our method trains three policies that, when chained, are capable of executing the task of transporting granular materials in both simulated and real-world scenarios, which existing popular deep reinforcement learning models fail to accomplish.

## I. INTRODUCTION

Imagine yourself coming back home from work, tired, hoping there is a robot to cook you a simple meal, or even just to help you put in ingredients. Yet, how long do we need to wait till a robot can simply use a spoon to pour some salt into a dish or some sugar into our coffee? Let alone the need to understand and manipulate rocks, sand or soil in places like construction sites, beaches, gardens, etc. Enabling a robot to manipulate granular materials is notably appealing and demanding. In response, this work takes a small step towards such challenging manipulation tasks, demonstrating the possibility of a robot learning to scoop and pour salts.

However, granular material manipulation is highly challenging. Firstly, accurately modelling the dynamics of granular materials with external contacts is highly difficult due to the infinite number of contacts, the plasticity treatment and the hardening process [1], which cause planning and learning-based manipulation to be highly expensive and intractable. Secondly, the high-dimensional state space of the grains poses formidable computational costs for sampling-based planning and exploration-based learning solutions [2].

Due to the difficulty of modelling granular materials, previous studies have predominantly relied on real-world

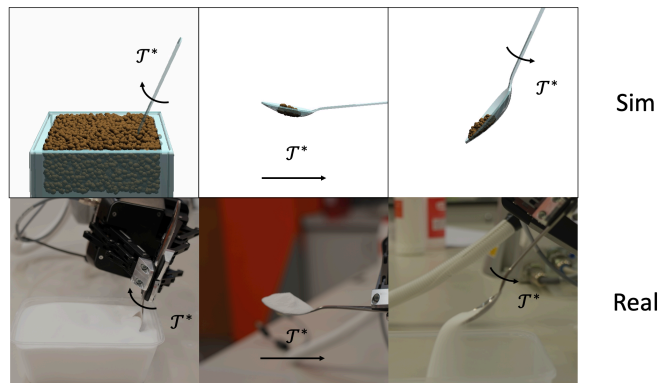


Fig. 1. Granular material manipulation in our simulator (*above*) and real environment (*below*). The agent manipulates a spoon to follow the optimal trajectory, completing the scooping, translating, and pouring sub-tasks.

sensor feedback [3]–[5], or deep learning (DL)-based dynamic models for state prediction [6], to learn manipulating granular materials. These approaches are typically time-consuming and computationally costly, without the guarantee of satisfactory real-world manipulation precision. Recent advances in GPU-accelerated parallel computation and continuum object simulation algorithms have shed light on the efficient and high-fidelity physics-based simulation of granular materials [7]. A typical example is the moving least-squares material point method (MLS-MPM) powered by the Taichi differentiable programming language [8], which has been used to develop simulators for manipulating soft bodies [9] and liquids [10]. The acceleration property and automatic differentiation (autodiff) capability of Taichi make it promising for application in the learning of granular material manipulation.

This work proposes a new framework, named **AutomaChef**, that is composed of a differentiable physics-based simulator, based on the MPM and Drucker-Prager (DP) yield criterion [1], coupled with a demonstration-guided learning framework. AutomaChef aims to address the problem of transporting granular materials in kitchen environments. Our learning framework includes off-policy reinforcement learning (RL) models, demonstration generation modules, and a signed distance field (SDF)-based collision detection module. The demonstrations are obtained by directly performing gradient-based optimisation through Taichi Autodiff. Instead of performing autodiff-based optimisation on granular materials directly, we use liquid for generating demonstrations, as optimisation on liquid is usually more stable, and the dynamic characteristics of liquid present high similarity to granular materials, thus transferable for providing demonstra-

Minglun Wei was supported by the UK Engineering and Physical Sciences Research Council (EPSRC) through a Doctoral Training Partnership (No. EP/W524682/1). This work was also partially supported by the EPSRC grant (No. EP/X018962/1). Corresponding author: Ze Ji.

<sup>1</sup>Minglun Wei, Xintong Yang, Seyed Amir Tafrihi, and Ze Ji are with the School of Engineering, Cardiff University, Cardiff, CF24 3AA, United Kingdom. WeiM9@cardiff.ac.uk; YangX66@cardiff.ac.uk; TafrihiSA@cardiff.ac.uk; JiZ1@cardiff.ac.uk

<sup>2</sup>Yu-Kun Lai is with the School of Computer Science and Informatics, Cardiff University, Cardiff, CF24 4AG, United Kingdom. LaiY4@cardiff.ac.uk

tion in our work. These automatically generated trajectories are used to assist the training of the RL policy, in the paradigm of learning from demonstrations (LfD), allowing rapid and effective learning that is challenging for classical RL models. Specifically, we conduct experiments with a robot to learn a three-stage manipulation task: using a spoon to scoop, transfer, and pour granular materials into a given area (see Fig. 1). Three corresponding policies, after training, are then linked together through the skill chaining method. In summary, our key contributions are as follows:

- A new robot learning framework is introduced for granular material manipulation based on differentiable simulation, allowing efficient RL-based learning through skill chaining, learning from liquid demonstrations, and collision detection.
- A differentiable simulator is built for robotic manipulation of granular material, based on the MPM and DP yield criterion, allowing efficient granular manipulation simulation and gradient-based trajectory optimisation. To our best knowledge, this is the first robot learning framework for granular manipulation built on a high-fidelity simulator.
- Our method for automatic generation of demonstrations accelerates the training process significantly and also avoids the high cost of human demonstrations.
- Both simulation and real-world experiments have been conducted, demonstrating superior performance achieved by the chained policies in the long-horizon multi-step scoop-transfer-pour task.

The remainder of the paper is organised as follows. Section II provides the background on granular material manipulation and simulation. Section III describes the proposed *AutomaChef* framework, followed by extensive experimental results in both simulated and real-world settings in Section IV. Section V concludes the work and discusses future work.

## II. RELATED WORK

### A. Real-Environment-Based Particle Manipulation

Manipulating liquid and granular materials is an active research area. An intuitive approach is to learn from real-world data. This can be in the form of learning from human demonstrations [11]. Many forms of real-world sensory feedback have been used, including visual information [3], [4], [12]–[15], external physical properties [14], [16], as well as auditory information [5]. For example, in [4], a Convolutional Neural Network (CNN) is proposed to predict future states using height maps computed from depth images of granular materials. In addition, [15] also incorporates density as an input for a CNN and employs RL models to enable the robot to gather or disperse granular materials on a surface. Rather than collecting feedback from RGB-D cameras, [5] leverages mechanical vibration information in the form of audio produced during the manipulation of granular materials. Using a learning framework based on CNN and Recurrent Neural Network (RNN), the robot is trained to execute shaking and dumping actions. These methods

neglect the interactions between particles, which inevitably impacts the results of robotic manipulation. Additionally, a more significant challenge is the excessive reliance on real-world data. Collecting data from the real environment and training learning models are both time-consuming processes.

### B. Simulation-Based Particle Manipulation

Some recent works have allowed robots to learn to manipulate materials through simulations. A common approach involves using trained DL models [6], [17]–[19] as surrogate models to approximate their physical properties. Graph Neural Network (GNN) is a popular choice due to its ability to represent particles and the physical properties between particles as nodes and edges. In [19], GNN is employed to simulate material dynamics and combined with prediction and control algorithms to enable liquid manipulation. [6] uses GNN to estimate the interactions between particles and a cup. The manipulation trajectory is then optimised through a population-based optimiser. Training such models typically requires a significant amount of data and time, and the simulation accuracy is often unsatisfactory. Moreover, any changes in the physical properties, such as friction angle, demand the regeneration of training data and retraining, imposing impracticalities. Other studies propose to learn by combining real-world data with low-resolution simulators. [20] integrates a likelihood-free Bayesian inference framework with a Discrete Element Methods (DEM) simulator, through which input depth images are used to infer material properties, allowing the robot to better learn granular material manipulation tasks. A low-fidelity simulator is used in [16] to simulate the physical properties of liquids and is combined with actual measurements to allow the robot to pour liquids into different containers and avoid spills. However, these learning processes still require multiple interactions between the agent and the environment.

### C. Physics Simulation for Granular Materials

One of the early methods for granular material simulation is to simulate the grains as individual entities [20]. However, tracking states and contacts for each grain poses a substantial computational burden [21]. As a hybrid Eulerian and Lagrangian method, the MPM was proposed to effectively capture particle dynamics with high visual details at a low cost. The hybrid nature of the MPM not only allows the use of Cartesian grids to efficiently handle collisions and fractures but also enables grid-based implicit integration [22]. MPM has been shown to excel in simulating plasticity and viscosity [23], [24]. Moreover, a hybrid method for granular material simulation that combines discrete and continuous processing is proposed to more accurately and efficiently simulate scenarios that previously required fully discrete processing [25]. When compared to other Lagrangian methods that also adopt the continuum assumption, MPM introduces stronger numerical viscosity [26] and simplifies the coupling of various materials. Furthermore, this method uses a continuous description of governing equations and easily incorporates user-controllable elastoplastic constitutive models. Despite

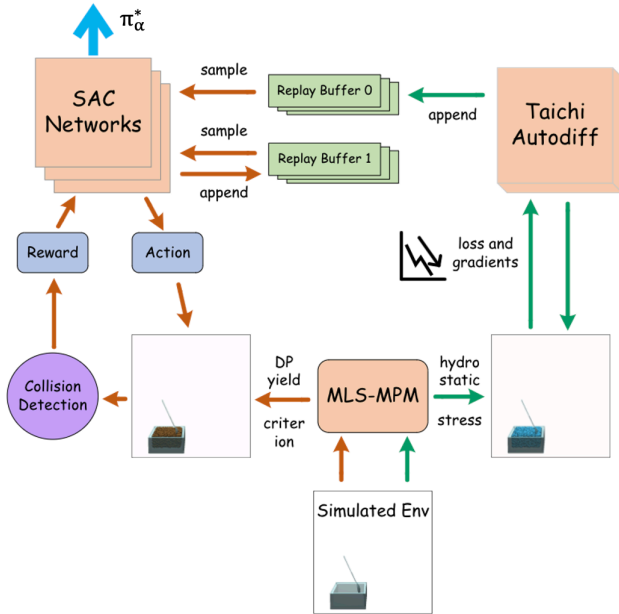


Fig. 2. Workflow of the proposed learning framework. Green arrows: imperfect demonstrations generated via gradient-based optimisation with a liquid dynamics model. Brown arrows: SAC training with dual replay buffers using demonstrations and data collected on the actual granular dynamics.

its remarkable capabilities, no learning framework has yet been proposed for robotic granular manipulation using this method.

### III. METHOD

The goal of this work is to develop an effective learning-based approach to granular material manipulation, showcasing a scenario of moving granular material from one container to the designated target area. Compared to previous studies [6], our learning framework aims at more complex tasks that require longer trajectories and comprise multiple sub-tasks: scooping, translating, and pouring. This section will describe the proposed framework, the physics-based simulator, and problem formulation.

#### A. Learning Framework

In our work, we propose a new learning-based framework for granular material manipulation. As depicted in Fig. 2, the framework is comprised of three main components, including 1) the RL model, which is a modified version of soft actor-critic (SAC), 2) Taichi Autodiff, which computes the demonstration trajectories through autodiff-based optimisation using Taichi, and 3) the physics-based simulator based on the MLS-MPM approach.

The RL models in our framework are based on the off-policy algorithm, SAC [27], which features an automatic temperature adjustment factor. We modified the original SAC by incorporating an additional replay buffer into the existing model, dedicated to storing demonstration data. This change is to address the issue that the demonstration data will be discarded from the replay buffer after a certain number of episodes, in the original version of SAC. Sampling from two replay buffers for training allows our model not only

to learn directly from expert demonstrations but also to maintain the ability to self-explore the environment. Notably, in our model, the demonstration data immediately impacts the network weights upon being placed into the replay buffer, thus accelerating the initialisation phase of the learning process. Additionally, in the original SAC algorithm, the policy network outputs the parameters of a Gaussian distribution used for sampling actions, which may struggle to capture the characteristics of the action distribution for complex sub-tasks. Hence, another innovation of ours involves modifying the output of the Gaussian policy in the complex scooping sub-task. By implementing linear transformations, we allow the policy network to match the actual action requirements in the environment more accurately.

The demonstration generation module is based on the Taichi Autodiff function. Given the intricacies of particle projection onto the DP yield surface in the principal stress space, it proves challenging to employ straightforward differentiation for gradient-based trajectory optimisation in granular material manipulation. The concept of transfer learning is utilised by incorporating gradient-optimised trajectories for manipulating liquid materials in specific scenarios as demonstrations in the RL framework. We define the weighted Manhattan distance  $DW$  from particles to target positions as the primary component of the loss function for our gradient-based trajectory optimisation:

$$DW_{\alpha}(i, j) = W_{\alpha}^x |x_i - x_j| + W_{\alpha}^y |y_i - y_j| + W_{\alpha}^z |z_i - z_j| \quad (1)$$

Considering that calculating the  $DW$  between all particles in the environment and the target position, especially in the scooping sub-task, would generate large gradients that would affect the optimisation. Therefore, we define the elite particle set  $\Upsilon$  within our framework as:

$$\Upsilon = \text{sort}(O_p, DW_s(i, goal))[: \tilde{N}_p^*] \quad (2)$$

where  $\tilde{N}_p^*$  is the number of elite particles,  $O_p$  denotes the particle observation state space for a single sub-task, and  $\text{sort}$  represents the function of sorting particles based on the  $DW$ , where the first  $\tilde{N}_p^*$  particles are selected. This implies that only  $\tilde{N}_p^*$  particles closest to the target position are utilised for calculating the loss during the optimisation of trajectories for manipulating liquid materials. This method of automatic demonstration generation eliminates the substantial costs associated with acquiring human demonstrations and also enables the possibility of forming a pipeline between the demonstration generation model and the demonstration-guided RL model. This streamlining facilitates an efficient learning process, allowing the RL models to benefit from automatically generated, high-quality demonstrations without the need for extensive human participation.

Drawing from the concept of skill chaining, the scooping sub-task, under the impetus of  $\mathcal{R}^{ea}$  (see details in Section III-C), is crafted to enable a smoother transition to the subsequent sub-task upon successful completion, thus creating a chain. Specifically, it is desirable for the robot to scoop the material and ensure the spoon is relatively levelled before

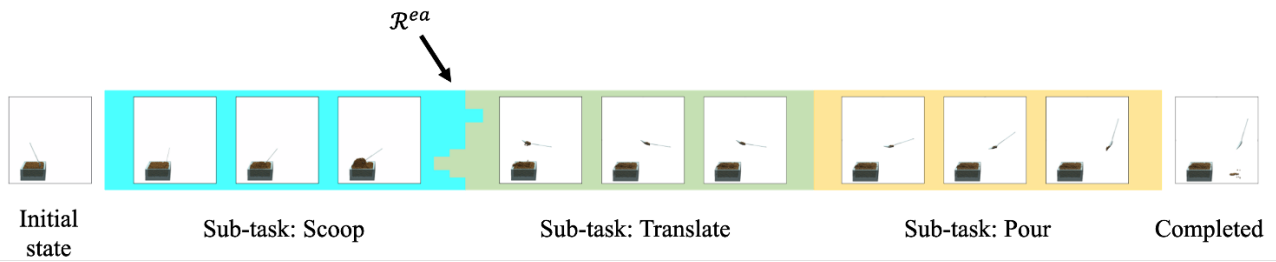


Fig. 3. Illustration of the problem setting. Our long-horizon complex task consists of three sub-tasks: scooping, translating, and pouring, with the aim of transporting granular material from a storage container to a target area. We employ the concept of skill chaining, innovatively integrating an Euler angle-based reward  $\mathcal{R}^{ea}$  within the learning paradigm of the scooping sub-task. This reward is designed to drive the agent towards achieving a seamless connection between scooping and translating actions.

transitioning to the translation motion. This arrangement allows the agent to accomplish complex tasks by seamlessly linking the actions across sub-tasks, as shown in Fig. 3.

Furthermore, our learning framework incorporates an SDF-based collision detection module that monitors the number of collisions between the tool manipulated and both granular particles and rigid-body particles at each timestep. For these particles, after determining their positions, the directed distance  $\vec{d}$  from the particles to the tool surface is calculated. When  $\vec{d}$  is less than or equal to zero, it indicates that the particle is located on or within the boundaries of the tool, signifying a collision has occurred.

### B. Physics-based Simulation of Granular materials

MPM is a method for simulating various materials, including solids, liquids, and gases. It uses Lagrangian elements, called material points, within a background mesh/grid for computations. For completeness, we describe the working principle of our physics-based simulator below. For more details about MPM and related techniques, please refer to [22].

**MLS-MPM:** As an improved element-free Galerkin method, MPM stores particle positions, velocities, deformation gradients, and mass on Lagrangian particles but uses a fixed Eulerian grid to handle interactions and calculate forces. Unlike the traditional MPM using B-spline basis functions, MLS-MPM employs MLS shape functions  $\Phi(\mathbf{x})$  as its basis functions, where  $\mathbf{x}$  are the locations. The efficiency of MLS-MPM stems from approximating the previously computed affine velocity matrix  $C_p^{n+1}$  as the Eulerian velocity gradient  $\nabla v^{n+1}$  during the update of particle-wise deformation gradient  $F_p$  in Lagrangian view. This leads to

$$F_p^{n+1} = (I + \Delta t C_p^{n+1}) F_p^n \quad (3)$$

where  $p$  and  $n$  denote particle quantities and timesteps [8].

**DP Yield Criterion:** The DP yield criterion, based on continuum mechanics and Coulomb friction, is used to realistically simulate the plasticity of large-scale free-flowing granular materials [1]. The amount of plastic deformation  $y(\sigma)$  can be calculated as:

$$y(\sigma) = \left\| \sigma - \frac{tr(\sigma)}{d} I \right\|_F + \frac{d\lambda + 2\mu}{2\mu} tr(\sigma) \sqrt{\frac{2}{3}} \frac{2 \sin \phi_f}{3 - \sin \phi_f} \quad (4)$$

where  $d$  represents the spatial dimension,  $\phi_f$  denotes the friction angle,  $\lambda$  and  $\mu$  are the Lamé constants of the material, and  $\sigma$  is the stress. If the stress lies within the yield surface, i.e.,  $y(\sigma) \leq 0$ , then the granular particles are not plasticised. Otherwise, depending on whether there is resistance to motion or dynamic friction, particles are projected onto the tip or side of the yield surface.

### C. Problem Formulation

Each sub-task in our work can be represented as a separate Markov decision process (MDP). Briefly, an MDP can be represented as a four-element tuple:  $(s_t, a_t, p(s_{t+1}|s_t, a_t), r(s_t, a_t))$ , where  $s_t$  and  $a_t$  denote the system state and the action at timestep  $t$ , respectively.  $p(s_{t+1}|s_t, a_t)$  is the transition probability function for reaching the next state  $s_{t+1}$  under the state  $s_t$  and action  $a_t$ .  $r(s_t, a_t)$  is the reward obtained after the state transition. To solve the MDP problems in our work, we adopt the SAC method, which optimises a stochastic policy and a soft Q function with an extra entropy maximisation term in the learning objective. The following subsections introduce the details of state/observation representation, action space, and rewards.

**States:** We define the state for each sub-task with three main components, including the states of the particles of granular material for the MPM-based simulation, the rigid objects in the environment, and the agent — that is, the end effector of the manipulator. A particle state matrix of size  $N_p \times d_p$  is employed to represent the state of the particles, where  $N_p$  is the total number of particles in the system and  $d_p$  is the dimensionality of state for each particle. In AutomaChef,  $d_p$  is set to 6, representing the position and velocity of a particle in the 3D Cartesian coordinates. To enable the agent to learn the ability to avoid collisions with containers, we decompose the container into rigid-body particles in the virtual environment and represent the states of rigid-body particles with an  $N_r \times d_r$  matrix, where  $N_r$  is the quantity of rigid-body particles. Since the rigid bodies are stationary,  $d_r$  is set to 3, including only the particle positions. Furthermore, a matrix of size  $N_a \times d_e$  is employed to encapsulate the state of the end effector. Here,  $N_a$  represents the number of agents, and  $d_e$  signifies the state dimension for each manipulator. In our case, there is one manipulator, hence  $N_a = 1$ . In general,  $d_e = 7$ , containing a 3D positional vector coupled with a 4D quaternion rotation vector, except

for the translation sub-task, where  $d_e$  is set to 3, as rotation is not needed in this case.

**Observations:** Optimising the observational input is essential for the learning models. Providing the model with state information on all particles may escalate complexity, thereby impeding the learning process. To address this issue, we introduce a parameter denoted by  $\delta_d$ , which serves as a tunable step size, facilitating systematic down-sampling of particles and rigid-body particles in the environment. Thus, combined with the state of the manipulator, the number of elements observed by the agent is:

$$N_o = \lfloor \frac{N_p}{\delta_d} \rfloor d_p + \lfloor \frac{N_r}{\delta_d} \rfloor d_r + N_a d_e \quad (5)$$

**Actions:** The agent in our work is capable of performing both linear translations and rotational actions. The actions are represented in a matrix of dimensions  $N_a \times d_a$ , where  $d_a$  signifies the dimensionality of action-related information. Beyond linear velocities along the Cartesian coordinate axes, the control of rotational dynamics is achieved through the update of angular velocities at the three Euler angles. Furthermore, in the RL models and environments, we impose boundaries  $A_{min}, A_{max} \in \mathbb{R}^{d_a}$ , on the selection of actions, contributing to enhancing system stability and efficiency to facilitate training.

**Rewards:** Each sub-task  $\alpha$  in AutomaChef is equipped with a unique reward function composed of multiple sub-rewards. Within the scope of the three sub-tasks, a distance-centric reward is integrated to serve as the principal incentive for the acquisition of granular material manipulation skills, which is operationalised by calculating the weighted Manhattan distance  $\mathcal{DW}$  between the manipulated particles and their target positions at each timestep  $t$ :

$$\mathcal{R}_\alpha^{dist}(t) = \beta_\alpha^{dist} (\gamma_\alpha^{dist} - \sum_{i=0}^{N_p^*} \mathcal{DW}_\alpha(\mathcal{P}_i^t, \mathcal{P}_{goal})) \quad (6)$$

where  $\mathcal{P}_i^t$  denotes the Cartesian coordinates of particle  $i$  at the time step  $t$ , while  $N_p^*$  represents the number of particles in the particle observation state space  $O_p$  for a single sub-task.  $\beta$  and  $\gamma$  are constants representing weights and biases, respectively. To facilitate a smoother transition between sub-tasks, an Euler angle reward is introduced to encourage the agent to have an appropriate posture, subsequent to the execution of each sub-task. This is achieved by extracting the 4D quaternion rotation vector  $\mathbf{q} = [q_w, q_x, q_y, q_z]$  of the agent at the end of the sub-task of the duration of  $T_s$ . The extracted vector is initially transformed into Euler angles  $\vartheta$ , constituting a set of Euler angles denoted as  $\Theta$ :

$$\begin{bmatrix} \vartheta^x \\ \vartheta^y \\ \vartheta^z \end{bmatrix} = \begin{bmatrix} \tan^{-1}(2(q_w q_x + q_y q_z), 1 - 2(q_x^2 + q_y^2)) \\ \sin^{-1}(2(q_w q_y - q_x q_z)) \\ \tan^{-1}(2(q_w q_z + q_x q_y), 1 - 2(q_y^2 + q_z^2)) \end{bmatrix} \quad (7)$$

where  $\vartheta$  represents Euler angles, and they form a set  $\Theta$ . The Euler angle reward is formulated as:

$$\mathcal{R}_\alpha^{ea} = \beta_\alpha^{ea} (\gamma_\alpha^{ea} - \sum_{j=0}^{N_a} \sum_{\vartheta \in \Theta} \mathcal{C}_r(\varepsilon_\vartheta) |\vartheta_{T_s-1}(j) - \vartheta_{goal}(j)|) \quad (8)$$

where  $\varepsilon$  and  $\mathcal{C}_r$  denote the adjustable rotation control vector and function to govern the rotational degrees of freedom across distinct sub-tasks. In the pouring sub-task, we introduce two sparse rewards to encourage and measure whether particles are poured out and whether they are poured into the designated area. In the pouring sub-task, we introduce two sparse rewards to encourage the agent to pour out particles and to accurately deposit them into the designated area. The reward function at timestep  $t$  for this sub-task is:

$$\begin{aligned} \mathcal{R}_p(t) = \mathcal{R}_p^{dist}(t) + \beta_p^p \Delta(T_s - 1) \mathcal{J}(P_i \in \Phi) \\ + \beta_p^t \sum_{i=0}^{N_p^*} \mathcal{J}(P'_i \in \Omega_p | P_i \in \Phi, P'_i \notin \Phi) \end{aligned} \quad (9)$$

where  $\Delta(T_s - 1)$  represents the Kronecker delta function  $\delta(t - T_s + 1)$ ,  $\mathcal{J} : X \rightarrow \{-1, 1\}$  is our defined indicator function,  $\Omega$  refers to the set of target positions,  $\Phi$  signifies the set of positions outside the environmental boundaries, and  $P'_i$  denotes the position of particle  $i$  at the last timestep. Given that the agent does not perform rotational actions in the translating sub-task, this implies that  $\varepsilon = [0, 0, 0]$ , and thus,  $\mathcal{R}_i^{ea}$  is disregarded. In its place, two sparse rewards are introduced to mitigate the transportation loss during the process and to encourage the transport of particles to the target area. The reward function of this sub-task is given by:

$$\begin{aligned} \mathcal{R}_t(t) = \mathcal{R}_t^{dist}(t) + \beta_t^n \sum_{i=0}^{N_p^*} \mathcal{I}(P_i \in \Phi | P'_i \notin \Phi) \\ + \beta_t^t \sum_{i=0}^{N_p^*} \Delta(T_s - 1) \mathcal{J}(P_i \in \Omega_t) \end{aligned} \quad (10)$$

where  $\mathcal{I}$  denotes the regular indicator function. In the scooping sub-task,  $\mathcal{R}_s^{dist}$ , which considers  $\mathcal{DW}$  for all particles in the container to the target position, tends to result in a low differential reward ratio between desired and undesired actions. This makes it challenging to influence results. Consequently, we incorporate the concept of elite particles mentioned in Eq. 2. Only  $\tilde{N}_p^*$  particles that are closest to the target positions are utilised for calculating  $\mathcal{R}_s^{dist}$  at each timestep. In order to avoid the results of the RL model optimisation falling into a local optimum, i.e., the agent prefers to choose not to perform rotational actions to avoid collisions, a reward is added to encourage the agent to interact with the particles. Besides the two sparse rewards in  $\mathcal{R}_t$ , another negative sparse reward is introduced to prevent collisions with the container. The reward function for scooping is defined as:

$$\begin{aligned} \mathcal{R}_s(t) = \mathcal{R}_s^{dist}(t) + \Delta(T_s - 1) (\beta_s^t \sum_{i=0}^{N_p^*} \mathcal{J}(P_i \in \Omega_s) + \mathcal{R}_s^{ea}) \\ + \beta_s^c \xi_t^c + \beta_s^n \sum_{i=0}^{N_p^*} \mathcal{I}(P_i \in \Phi | P'_i \notin \Phi) + \beta_s^i \mathcal{I}(\xi_t^r > 0) \end{aligned} \quad (11)$$

where  $\xi_t^r$  and  $\xi_t^c$  denote the number of rigid-body particles and particles that collide with the agent at timestep  $t$ . Within



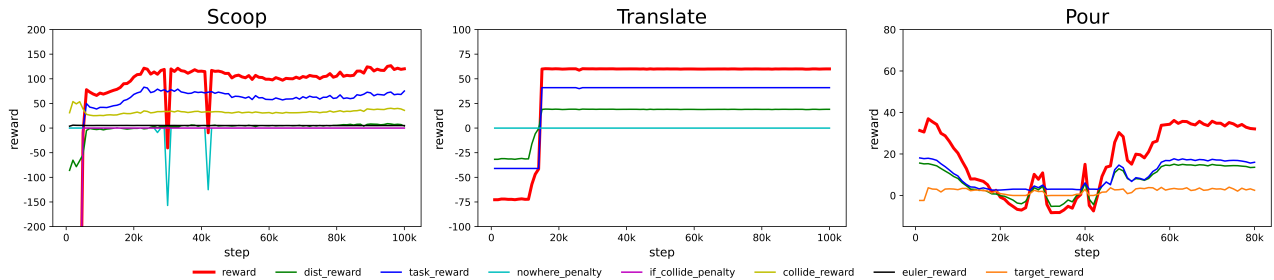


Fig. 4. The variation in rewards for each sub-task under training with our DG-SAC models is depicted. The total rewards are highlighted in red and bolded for emphasis. To better showcase the performance, we only capture rewards above -200 during the training of the scooping sub-task.

all the reward functions,  $\beta$  and  $\gamma$  are constants representing weights and biases, respectively, and among them,  $\beta^n$  and  $\beta^i$  are negative values.

#### IV. EXPERIMENTS AND RESULTS

This section first introduces the configurations of our physical simulator and RL models. Then, the training results of the proposed demonstration-guided SAC (DG-SAC) are shown next and compared with the Proximal Policy Optimisation (PPO) and SAC as baselines. The objectives of our experiments include: 1) verifying if our method can successfully transport granular materials into a target area; 2) assessing the effectiveness of the DG-SAC method; and 3) evaluating the performance of the simulation-trained policies in a real-world setup.

##### A. Experimental Setup

Utilising Taichi, we employ the MLS-MPM along with the DP yield criterion for the simulation of granular materials. A  $1 \times 1 \times 1$  m simulation environment is created for the proposed task. Within the environments, the end-effector tool, which is the spoon, and the containers, are modelled as 3D meshes. The containers in certain environments are also populated with and substituted by rigid-body particles. Each of the three sub-tasks has a duration of 1000 timesteps, and a total of 16,640 granular material particles are created in simulation in the environment. In the simulation experiments, we assume the friction angle and Lamé constants of the granular material employed are  $\phi_f = 30^\circ$ ,  $\mu = 416.67$ , and  $\lambda = 277.78$  respectively.

We employ two efficient and state-of-the-art RL algorithms, PPO and SAC, to serve as the baselines for benchmarking our RL model, DG-SAC. Furthermore, we conducted an ablation study on our proposed model to examine the impact of incorporating the demonstration replay buffer during training. For clarity, we define this policy as DGN-SAC, denoting the policy model without using the additional demonstration replay buffer here. The distinction between DGN-SAC and SAC lies in that DGN-SAC has its network parameters' weights updated during the process of adding demonstrations prior to training.

Tables I and II show the parameters of the SAC and PPO models. For the demonstration generation module, we employ the Adam optimiser for gradient-based trajectory optimisation, with a learning rate of 0.0001. Our RL learning framework, based on a physical simulator, is trained on a

desktop computer equipped with an Nvidia RTX 3080 GPU and an Intel i7-12700K CPU.

TABLE I

SAC PARAMETERS	
gamma	0.99
policy lr	0.003
entropy lr	0.003
batch size	128
replay buffer 0 size	5e4
replay buffer 1 size	1e5
hidden layers	2

TABLE II

PPO PARAMETERS	
gamma	0.99
entropy coef	0.01
gae lambda	0.95
alpha	0.99
clip parameter	0.2

##### B. Simulation Results

For each proposed sub-task, training was performed over a spectrum of 80,000 to 100,000 simulation steps based on varying levels of task difficulties, employing PPO, SAC, DGN-SAC, and our DG-SAC model. Table III shows the rewards obtained from the training. We conducted five training tests for each sub-task, using each model separately. Due to fluctuations in the reward values, we selected the average reward over the last 10,000 timesteps prior to the end of the training as the reward here. In addition to the accumulated reward per episode, we defined a specific target reward to quantitatively assess task completion. For the pouring and translating sub-tasks, the target reward includes all sparse reward components in Eqs. 9 and 10, excluding  $\mathcal{R}_\alpha^{dist}$  that drives the agent to complete the task at every timestep. For the scooping sub-task, the target reward refers to all the sparse components in Eq. 11, excluding  $\mathcal{R}_s^{dist}$  and  $\beta_s^c \xi_t^p$ . Overall, the target rewards are used to assess whether the particles are poured into a specified region, whether the particles are translated to a specified position, and whether sufficient amounts of particles are scooped up without colliding with the container and within the boundary. The experimental results in Table III reveal that our demonstration-guided RL framework exhibits outstanding performance across three sub-tasks of varying difficulty levels.

As shown in Table III, due to the high difficulty level of the scooping sub-task, the PPO models incur significant negative rewards caused by frequent collisions with the container, leading to confusion for the training process. On the other hand, although we introduced a sub-reward  $\beta_s^c \xi_t^p$  in our reward function designed to encourage the agent to interact with particles, the SAC model was found to be more impacted by the negative rewards caused by the collisions with

TABLE III

THE REWARD (ABOVE) AND TARGET REWARD (BELOW) WITH THEIR STANDARD DEVIATIONS FOR EACH EVALUATION METHOD.

Task	Scoop	Translate	Pour
PPO	-2870.91±44.57	-75.04±4.49	<b>474.55±287.67</b>
SAC	-74.12±8.57	-72.66±0.09	339.79±13.89
DGN-SAC	47.48±19.15	3.12±24.29	-85.88±15.56
DG-SAC (Ours)	<b>110.60±9.53</b>	<b>60.01±0.05</b>	222.26±91.74

Task	Scoop	Translate	Pour
PPO	-2799.09±44.61	-41.00±0.00	14.24±19.60
SAC	-6.22±4.79	-41.00±0.00	13.60±12.91
DGN-SAC	35.34±3.69	-8.90±19.00	-30.45±0.00
DG-SAC (Ours)	<b>63.64±10.78</b>	<b>41.00±0.00</b>	<b>26.06±6.79</b>

the container. Consequently, the SAC policy tends to produce a small angular velocity on the learned policies, resulting in failing to complete the task, and converge to a locally optimal solution. The DGN-SAC model, while capable of learning the scooping action within a limited training set, does not scoop a sufficient number of particles. In fact, the difficulty in training the scooping action is primarily related to the unavoidable sparsity of rewards, which is largely due to the introduction of the collision penalty. For instance, an agent might successfully complete the scooping task in one training episode, receiving a substantial reward, but may incur a large negative penalty in the next episode due to a collision with the container. This penalty cannot be structured as a continuous reward, and, if set too low, the agent will pass through the container to complete the task, which is obviously against common sense.

Our model, DG-SAC, significantly outperforms other models in terms of both cumulative rewards during the training process and the target rewards used to evaluate task completion. Fig. 4 illustrates the composition of individual reward components for our model across the three sub-tasks during a single training process. Our model, despite receiving negative rewards due to collisions with the container, can quickly recover and succeed in scooping up particles without colliding. Subsequently, although negative rewards are incurred in two episodes due to particles moving out of bounds during the exploration process, it swiftly corrected these errors and converged to a high target reward value.

Furthermore, to validate the effectiveness of our designed skill chaining structure, we present in Table IV the variations in the Euler angles of the agent of our model on the end timestep of the scooping sub-task over multiple trials under the stimulus of reward  $\mathcal{R}^{ea}$ . The agent is expected to achieve a change of  $-120$  degrees along the direction of  $\vartheta^z$  before the completion of scooping to better facilitate the transition to the subsequent translating sub-task. Experiments demonstrate that our learning framework can effectively learn tasks with complex reward structures and enable seamless integration within a small margin of error.

For the translating sub-task, our model exhibits superior performance, successfully transporting all particles to the target location in all five trials. In contrast, within the

TABLE IV

THE VARIATIONS OF THE EULER ANGLE OF THE AGENT AND THEIR RELATIVE ERRORS TO THE TARGET VALUE AT THE TRANSITION BETWEEN THE SCOOPING AND TRANSLATING SUB-TASKS.

Task	Target	Result	Relative Error
Scoop	-120	-123.77±0.96	3.14%±0.8%

corresponding training episodes, the PPO and SAC models failed to transport any particles. This excellent performance is mainly attributed to the high-quality demonstrations provided. Due to the different physical properties of liquids and granular materials, the gradient-optimised trajectories for scooping up and pouring liquids do not achieve high target rewards when used to scoop or pour granular materials. However, this issue did not arise in the process of training the translating sub-task, as the policy for moving liquid also applies to the case of moving granular materials without scattering any granular particles. This could be due to the presence of the Coulomb friction.

For the most straightforward task of pouring, PPO, which excels at training simple tasks, often yields results with significant cumulative rewards. This is attributed to the rapid pouring of particles soon after the task commences. However, the training results using this model lack stability, as reflected in the high standard deviation of the target rewards. In comparison, our method exhibits a higher mean in target rewards as well as greater stability.

Overall, our demonstration-guided RL framework demonstrates significantly superior capability and stability in simulation environments. Given the complexity and specificity of the tasks, conventional model-free RL models struggle to achieve stable convergence in these tasks.

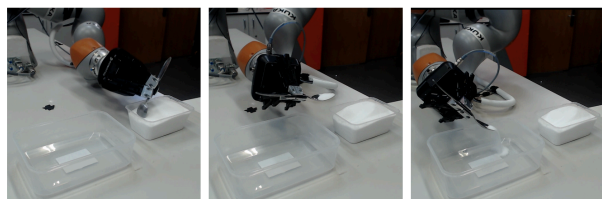


Fig. 5. A sequence of snapshots showing our real robot successfully completed the task of transporting granular materials between two containers.

### C. Real-World Manipulation

To verify the performance of our method in real-world environments, we conducted real-robot experiments on manipulating granular materials. As shown in Fig. 5, these experiments were carried out on a seven-degree-of-freedom robot manipulator, Kuka iiwa, equipped with a ROBOTIQ 3-finger robot gripper to complete the complex task we proposed. Salt, sugar, and flour, as common granular materials in kitchen scenarios, are selected as the materials for our manipulation experiments. Additionally, our experimental setup comprises one container for storing granular materials and another container to serve as the target zone. Given the inherent properties of granular materials, which complicate quantitative analysis in real-world settings, we define the

criterion for successfully completing the task as the visually confirmed transfer of granular materials into the target container without colliding with both containers. We conducted tests using the optimal trajectories obtained from our simulated environment and undertook three experiments for the three types of granular materials mentioned above. The robot successfully accomplished all tasks without colliding with the container in all the trials. This result highlights the effectiveness and feasibility of our method for transferring learned skills from simulated to real-world settings.

## V. CONCLUSIONS

In this paper, we propose a new learning framework, AutomaChef, for granular material manipulation. A differentiable simulator is built in the work based on the MLS-MPM and the DP yield criterion, which allow robots to perform complex tasks of transferring granular materials. In our constructed simulated environment, the agent learns to perform three sub-tasks that together constitute a complex, long-horizon task. Our learning framework incorporates a collision detection module and employs the concept of skill chaining. These features are designed to enable the agent to avoid obstacles and seamlessly transition between the three sub-tasks. In addition, our learning framework incorporates automatically generated demonstrations into the SAC model. Experimental results demonstrate that the optimal trajectories trained by our model excel at accomplishing the proposed complex task in both simulated and real-world environments. Furthermore, our proposed DG-SAC model trains policies to converge on the desired solutions while maintaining stability throughout the process. However, there are certain limitations. Bridging the gap between simulated and real environments remains a primary challenge to be addressed in the future. Additionally, we hope to extend AutomaChef to more complex scenarios, necessitating our learning framework to exhibit improved generalisability.

## REFERENCES

- [1] G. Klár, T. Gast, A. Pradhana, C. Fu, C. Schroeder, C. Jiang, and J. Teran, "Drucker-prager elastoplasticity for sand animation," *ACM Transactions on Graphics (TOG)*, vol. 35, no. 4, pp. 1–12, 2016.
- [2] X. Lin, Y. Wang, J. Olkin, and D. Held, "Softgym: Benchmarking deep reinforcement learning for deformable object manipulation," in *Conference on Robot Learning*, pp. 432–448, PMLR, 2021.
- [3] K. Takahashi, W. Ko, A. Ummadisingu, and S.-i. Maeda, "Uncertainty-aware self-supervised target-mass grasping of granular foods," in *2021 IEEE International Conference on Robotics and Automation (ICRA)*, pp. 2620–2626, IEEE, 2021.
- [4] C. Schenck, J. Tompson, S. Levine, and D. Fox, "Learning robotic manipulation of granular media," in *Conference on Robot Learning*, pp. 239–248, PMLR, 2017.
- [5] S. Clarke, T. Rhodes, C. G. Atkeson, and O. Kroemer, "Learning audio feedback for estimating amount and flow of granular material," *Proceedings of Machine Learning Research*, vol. 87, 2018.
- [6] N. Tuomainen, D. Blanco-Mulero, and V. Kyrki, "Manipulation of granular materials by learning particle interactions," *IEEE Robotics and Automation Letters*, vol. 7, no. 2, pp. 5663–5670, 2022.
- [7] Y. Fei, Q. Guo, R. Wu, L. Huang, and M. Gao, "Revisiting integration in the material point method: a scheme for easier separation and less dissipation," *ACM Transactions on Graphics (TOG)*, vol. 40, no. 4, pp. 1–16, 2021.

- [8] Y. Hu, Y. Fang, Z. Ge, Z. Qu, Y. Zhu, A. Pradhana, and C. Jiang, "A moving least squares material point method with displacement discontinuity and two-way rigid body coupling," *ACM Transactions on Graphics (TOG)*, vol. 37, no. 4, pp. 1–14, 2018.
- [9] Z. Huang, Y. Hu, T. Du, S. Zhou, H. Su, J. B. Tenenbaum, and C. Gan, "Plasticinelab: A soft-body manipulation benchmark with differentiable physics," *arXiv preprint arXiv:2104.03311*, 2021.
- [10] Z. Xian, B. Zhu, Z. Xu, H.-Y. Tung, A. Torralba, K. Fragkiadaki, and C. Gan, "Fluidlab: A differentiable environment for benchmarking complex fluid manipulation," *arXiv preprint arXiv:2303.02346*, 2023.
- [11] Y. Huang, J. Wilches, and Y. Sun, "Robot gaining accurate pouring skills through self-supervised learning and generalization," *Robotics and Autonomous Systems*, vol. 136, p. 103692, 2021.
- [12] C. Schenck and D. Fox, "Visual closed-loop control for pouring liquids," in *2017 IEEE International Conference on Robotics and Automation (ICRA)*, pp. 2629–2636, IEEE, 2017.
- [13] C. Do and W. Burgard, "Accurate pouring with an autonomous robot using an rgb-d camera," in *Intelligent Autonomous Systems 15: Proceedings of the 15th International Conference IAS-15*, pp. 210–221, Springer, 2019.
- [14] T. Lopez-Guevara, R. Pucci, N. K. Taylor, M. U. Gutmann, S. Ramamoorthy, and K. Suhr, "Stir to pour: Efficient calibration of liquid properties for pouring actions," in *2020 IEEE/RSJ International Conference on Intelligent Robots and Systems (IROS)*, pp. 5351–5357, IEEE, 2020.
- [15] Y. Zhang, W. Yu, C. K. Liu, C. Kemp, and G. Turk, "Learning to manipulate amorphous materials," *ACM Transactions on Graphics (TOG)*, vol. 39, no. 6, pp. 1–11, 2020.
- [16] T. L. Guevara, N. K. Taylor, M. Gutmann, S. Ramamoorthy, and K. Suhr, "Adaptable pouring: Teaching robots not to spill using fast but approximate fluid simulation," in *1st Conference on Robot Learning 2017*, pp. 77–86, 2017.
- [17] B. Ummenhofer, L. Prantl, N. Thuerey, and V. Koltun, "Lagrangian fluid simulation with continuous convolutions," in *International Conference on Learning Representations*, 2019.
- [18] Y. Shao, C. C. Loy, and B. Dai, "Transformer with implicit edges for particle-based physics simulation," in *European Conference on Computer Vision*, pp. 549–564, Springer, 2022.
- [19] Y. Li, J. Wu, R. Tedrake, J. B. Tenenbaum, and A. Torralba, "Learning particle dynamics for manipulating rigid bodies, deformable objects, and fluids," *arXiv preprint arXiv:1810.01566*, 2018.
- [20] C. Matl, Y. Narang, R. Bajcsy, F. Ramos, and D. Fox, "Inferring the material properties of granular media for robotic tasks," in *2020 IEEE International Conference on Robotics and Automation (ICRA)*, pp. 2770–2777, IEEE, 2020.
- [21] P. A. Cundall and O. D. Strack, "A discrete numerical model for granular assemblies," *geotechnique*, vol. 29, no. 1, pp. 47–65, 1979.
- [22] C. Jiang, C. Schroeder, J. Teran, A. Stomakhin, and A. Selle, "The material point method for simulating continuum materials," in *Acm siggraph 2016 courses*, pp. 1–52, 2016.
- [23] M. Gao, A. P. Tampubolon, C. Jiang, and E. Sifakis, "An adaptive generalized interpolation material point method for simulating elastoplastic materials," *ACM Transactions on Graphics (TOG)*, vol. 36, no. 6, pp. 1–12, 2017.
- [24] X. Han, T. F. Gast, Q. Guo, S. Wang, C. Jiang, and J. Teran, "A hybrid material point method for frictional contact with diverse materials," *Proceedings of the ACM on Computer Graphics and Interactive Techniques*, vol. 2, no. 2, pp. 1–24, 2019.
- [25] Y. Yue, B. Smith, P. Y. Chen, M. Chantharayukhonthorn, K. Kamrin, and E. Grinspun, "Hybrid grains: Adaptive coupling of discrete and continuum simulations of granular media," *ACM Transactions on Graphics (TOG)*, vol. 37, no. 6, pp. 1–19, 2018.
- [26] T. Yang, J. Chang, M. C. Lin, R. R. Martin, J. J. Zhang, and S.-M. Hu, "A unified particle system framework for multi-phase, multi-material visual simulations," *ACM Transactions on Graphics (TOG)*, vol. 36, no. 6, pp. 1–13, 2017.
- [27] T. Haarnoja, A. Zhou, P. Abbeel, and S. Levine, "Soft actor-critic: Off-policy maximum entropy deep reinforcement learning with a stochastic actor," in *International conference on machine learning*, pp. 1861–1870, PMLR, 2018.